DESY 99-192
RAL-TR-99-083
February 2000

Double Higgs production at TeV Colliders in the Minimal Supersymmetric Standard Model

R. Lafaye[1], D.J. Miller[2], M. Mühlleitner[2] and S. Moretti[3]

1) Laboratoire d'Annecy-le-Vieux de Physique des Particules (LAPP), B.P. 110, F-74941 Annecy-le-Vieux CEDEX, France.

2) Deutsches Elektronen-Synchrotron (DESY), Notkestrasse 85, D-22603 Hamburg, Germany.

3) Rutherford Appleton Laboratory (RAL), Chilton, Didcot, Oxon OX11 0QX, United Kingdom.

Contribution to the Workshop 'Physics at TeV Colliders', Les Houches, France, 8–18 June 1999 (to appear in the proceedings)

Abstract

The reconstruction of the Higgs potential in the Minimal Supersymmetric Standard Model (MSSM) requires the measurement of the trilinear Higgs self-couplings. The 'double Higgs production' subgroup has been investigating the possibility of detecting signatures of processes carrying a dependence on these vertices at the Large Hadron Collider (LHC) and future Linear Colliders (LCs). As reference reactions, we have chosen $gg \to hh$ and $e^+e^- \to hhZ$, respectively, where h is the lightest of the MSSM Higgs bosons. In both cases, the Hhh interaction is involved. For $m_H \gtrsim 2m_h$, the two reactions are resonant in the $H \to hh$ mode, providing cross sections which are detectable at both accelerators and strongly sensitive to the strength of the trilinear coupling involved. We explore this mass regime of the MSSM in the $h \to b\bar{b}$ decay channel, also accounting for irreducible background effects.

1 Introduction

Considerable attention has been devoted to double Higgs boson production at future e^+e^- and hadron colliders, both in the Standard Model (SM) and the MSSM [1, 2, 3]. For the SM, detailed signal-to-background studies already exist for a LC environment [3], for both 'reducible' and 'irreducible' backgrounds [4, 5], which have assessed the feasibility of experimental analyses. At the LHC, since here the typical SM signal cross sections are of the order of 10 fb [2], high integrated luminosities would be needed to generate a statistically large enough sample of double Higgs events. These would be further obscured by an overwhelming background, making their selection and analysis in a hadronic environment extremely difficult. Thus, in this contribution we will concentrate only on the case of the MSSM.

In the Supersymmetric (SUSY) scenario, the phenomenological potential of these reactions is two-fold. Firstly, in some specific cases, they can furnish new discovery channels for Higgs bosons. Secondly, they are all dependent upon several triple Higgs self-couplings of the theory, which can then be tested by comparing theoretical predictions with experimental measurements. This is the first step in the reconstruction of the Higgs potential itself[1].

The Higgs Working Group (WG) has focused much of its attention in assessing the viability of these reactions at future TeV colliders. However, the number of such processes is very large both at the LHC and a LC [2, 3], so only a few 'reference' reactions could be studied in the context of this Workshop. Work is in progress for the longer term, which aims to cover most of the double Higgs production and decay phenomenology at both accelerators [6].

These reference reactions were chosen to be $gg \to hh$ for the LHC (see top of Fig. 1) and $e^+e^- \to hhZ$ for the LC (see bottom of Fig. 1), where h is the lightest of the MSSM scalar Higgs bosons. The reason for this preference is simple. Firstly, a stable upper limit exists on the value of m_h, of the order of 130 GeV, now at two-loop level [7], so that its detection is potentially well within the reach of both the LHC and a LC. In contrast, the mass of all other Higgs bosons of the MSSM may vary from the electroweak (EW) scale, $\mathcal{O}(m_Z)$, up to the TeV region. In addition, as noted in Ref. [2], the multi-b final state in $gg \to hh \to b\bar{b}b\bar{b}$, with two resonances and large transverse momenta, may be exploited in the search for the h scalar in the large $\tan\beta$ and moderate m_A region. This is a corner of the MSSM parameter space that has so far eluded the scope of the standard Higgs production and decay modes [8]. (The symbol A here denotes the pseudoscalar Higgs boson of the MSSM, and we reserve the notation H for the heaviest scalar Higgs state of the model.) However, this paper will not investigate the LHC discovery potential in this mode, given the very sophisticated treatment of the background (well beyond the scope of this note) required by the assumption that no h scalar state has been previously discovered (see below). This will be done in Ref. [6]. Furthermore, the $gg \to hh$ and $e^+e^- \to hhZ$ modes largely dominate double Higgs production [2, 3], at least for centre-of-mass (CM) energies of 14 TeV at the LHC and 500 GeV in the case of a LC, the default values of our analysis. (Notice that we assume no polarization of the incoming beams in e^+e^- scatterings.) Finally, when $m_H \gtrsim 2m_h$, the two reactions are resonant, as they can both proceed via intermediate states

[1]The determination of the quartic self-interactions is also required, but appears out of reach for some time: see Refs. [2, 3] for some cross sections of triple Higgs production.

gg to double Higgs fusion at the LHC: $gg \to hh$

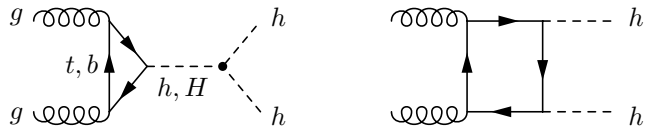

double Higgs-strahlung at a LC: $e^+e^- \to hhZ$

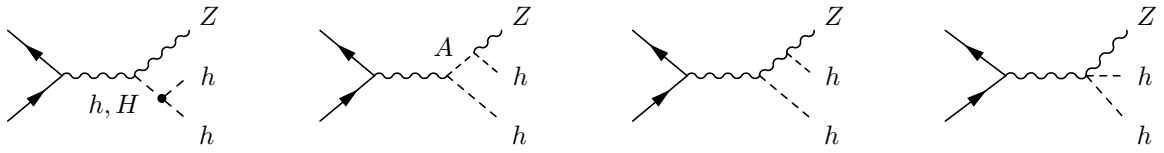

Figure 1: Diagrams contributing to $gg \to hh$ (top) and $e^+e^- \to hhZ$ (bottom) in the MSSM.

involving H scalars, through $gg \to H$ and $e^+e^- \to HZ$, which in turn decay via $H \to hh$ [9]. Thus, the production cross sections are largely enhanced [2, 3] (up to two orders of magnitude above typical SM rates at the LHC [2]) and become clearly visible. This allows the possibility of probing the trilinear Hhh vertex at one or both these colliders.

The dominant decay rate of the MSSM h scalar is into $b\bar{b}$ pairs, regardless of the value of $\tan\beta$ [9]. Therefore, the final signatures of our reference reactions always involve four b-quarks in the final state. (In the case of a LC environment, a further trigger on the accompanying Z boson can be exploited.)

If one assumes very efficient tagging and high-purity sampling of b-quarks, the background to hh events at the LHC is dominated by the irreducible QCD modes [10]. Among these, we focus here on the cases $q\bar{q}, gg \to b\bar{b}b\bar{b}$, as representative of ideal b-tagging performances. These modes consist of a purely QCD contribution of $\mathcal{O}(\alpha_s^4)$, an entirely EW process of $\mathcal{O}(\alpha_{em}^4)$ (with no double Higgs intermediate states) and an $\mathcal{O}(\alpha_s^2\alpha_{em}^2)$ component consisting of EW and QCD interactions. (Note that in the EW case only $q\bar{q}$ initiated subprocesses are allowed at tree-level.) For a LC, the final state of the signal is $b\bar{b}b\bar{b}Z$, with the Z reconstructed from its decay products in some channel. Here, the EW background is of $\mathcal{O}(\alpha_{em}^5)$ away from resonances (and, again, contains no more than one intermediate Higgs boson), whereas the EW/QCD background is proportional to $(\alpha_s^2\alpha_{em}^3)$.

In general, EW backgrounds can be problematic due to the presence of Z vectors and single Higgs scalars yielding $b\bar{b}$ pairs, with the partons being typically at large transverse momenta and well separated. In contrast, the QCD backgrounds involve no heavy objects decaying to $b\bar{b}$ pairs and are dominated by the typical infrared (i.e., soft and collinear) QCD behaviour of the partons in the final state. However, they can yield large production rates because of the strong couplings.

In this study, we investigate the interplay between the signal and background at both colliders, adopting detector as well as dedicated selection cuts. We carry out our analysis

at both parton and hadron level. The plan of this note is as follows. The next Section details the procedure adopted in the numerical computation. Sect. 3 displays our results and contains our discussion. Finally, in the last section, we summarise our findings and consider possible future studies.

2 Calculation

For the parton level simulation, the double Higgs production process at the LHC, via gg fusion, has been simulated using the program of Ref. [11] to generate the interaction $gg \to hh$, with the matrix elements (MEs) taken at leading-order (LO) for consistency with our treatment of the background. We then perform the two $h \to b\bar{b}$ decays to obtain the actual $4b$-final state. For double Higgs production at a LC, we use a source code for the signal derived from that already used in Ref. [5]. At both colliders, amplitudes for background events were generated by means of MadGraph [12] and the `HELAS` package [13]. Note that interferences between signal and backgrounds, and between the various background contributions themselves, have been neglected. This is a good approximation for the interferences involving the signal because of the very narrow width of the MSSM lightest Higgs boson. Similarly, the various background subprocesses have very different topologies, and one would expect their interferences to be small in general.

The Higgs boson masses and couplings of the MSSM can be expressed at tree-level in terms of the mass of the pseudoscalar Higgs state, m_A, and the ratio of the vacuum expectation values of the two neutral fields in the two iso-doublets, $\tan\beta$. At higher order however, top and stop loop-effects can become significant. Radiative corrections in the one-loop leading m_t^4 approximation are parameterised by

$$\epsilon \approx \frac{3G_F m_t^4}{\sqrt{2}\pi^2 \sin^2\beta} \log\frac{m_S^2}{m_t^2} \tag{1}$$

where the SUSY breaking scale is given by the common squark mass, m_S, set equal to 1 TeV in the numerical analysis. If stop mixing effects are modest at the SUSY scale, they can be accounted for by shifting m_S^2 in ϵ by the amount $\Delta m_S^2 = \hat{A}^2[1 - \hat{A}^2/(12m_S^2)]$ ($\hat{A}$ is the trilinear common coupling). The charged and neutral CP-even Higgs boson masses, and the Higgs mixing angle α are given in this approximation by the relations:

$$\begin{aligned}
m_{H^\pm}^2 &= m_A^2 + m_Z^2\cos^2\theta_W, \\
m_{h,H}^2 &= \tfrac{1}{2}[m_A^2 + m_Z^2 + \epsilon \\
&\mp \sqrt{(m_A^2 + m_Z^2 + \epsilon)^2 - 4m_A^2 m_Z^2\cos^2 2\beta - 4\epsilon(m_A^2\sin^2\beta + m_Z^2\cos^2\beta)}], \\
\tan 2\alpha &= \tan 2\beta \frac{m_A^2 + m_Z^2}{m_A^2 - m_Z^2 + \epsilon/\cos 2\beta} \qquad \text{with} \qquad -\frac{\pi}{2} \le \alpha \le 0,
\end{aligned} \tag{2}$$

as a function of m_A and $\tan\beta$. The triple Higgs self-couplings of the MSSM can be parameterised [14, 15] in units of M_Z^2/v, $v = 246$ GeV, as,

$$\lambda_{hhh} = 3\cos 2\alpha \sin(\beta+\alpha) + 3\frac{\epsilon}{m_Z^2}\frac{\cos\alpha}{\sin\beta}\cos^2\alpha,$$

$$
\begin{aligned}
\lambda_{Hhh} &= 2\sin 2\alpha \sin(\beta+\alpha) - \cos 2\alpha \cos(\beta+\alpha) + 3\frac{\epsilon}{m_Z^2}\frac{\sin\alpha}{\sin\beta}\cos^2\alpha, \\
\lambda_{HHh} &= -2\sin 2\alpha \cos(\beta+\alpha) - \cos 2\alpha \sin(\beta+\alpha) + 3\frac{\epsilon}{m_Z^2}\frac{\cos\alpha}{\sin\beta}\sin^2\alpha, \\
\lambda_{HHH} &= 3\cos 2\alpha \cos(\beta+\alpha) + 3\frac{\epsilon}{m_Z^2}\frac{\sin\alpha}{\sin\beta}\sin^2\alpha, \\
\lambda_{hAA} &= \cos 2\beta \sin(\beta+\alpha) + \frac{\epsilon}{m_Z^2}\frac{\cos\alpha}{\sin\beta}\cos^2\beta, \\
\lambda_{HAA} &= -\cos 2\beta \cos(\beta+\alpha) + \frac{\epsilon}{m_Z^2}\frac{\sin\alpha}{\sin\beta}\cos^2\beta. \qquad (3)
\end{aligned}
$$

Next-to-leading order (NLO) effects are certainly dominant, though the next-to-next-to-leading order (NNLO) ones cannot entirely be neglected (especially in the Higgs mass relations). Thus, in the numerical analysis, the complete one-loop and the leading two-loop corrections to the MSSM Higgs masses and the triple Higgs self-couplings are included. The Higgs masses, widths and self-couplings have been computed using the HDECAY program described in Ref. [16], which uses a running b-mass in evaluating the $h \to b\bar{b}$ decay fraction. Thus, for consistency, we have evolved the value of m_b entering the hbb Yukawa couplings of the $h \to b\bar{b}$ decay currents of our processes in the same way.

For our analysis, we have considered $\tan\beta = 3$ and 50. For the LHC, high values of $\tan\beta$ produce a signal cross section much larger than the $\tan\beta = 3$ scenario, over almost the entire range of m_A. However, this enhancement is due to the increase of the down-type quark-Higgs coupling, which is proportional to $\tan\beta$ itself, and serves only to magnify the dominance of the quark box diagrams of Fig. 1. Unfortunately, these graphs have no dependence on either of the two triple Higgs self-couplings entering the gluon-gluon process considered here, i.e., λ_{hhh} and λ_{Hhh}. Thus, although the cross section is comfortably observable, all sensitivity to such vertices is lost. Therefore, the measurement of the triple Higgs self-coupling, λ_{Hhh}, is only feasible at the LHC for low $\tan\beta$ due to the resonant production of the heavy Higgs boson (see Fig. 5a of Ref. [2]).

In contrast, the cross section for double Higgs production at the LC is small for large $\tan\beta$ because there is no heavy Higgs resonance (see Fig. 8 of Ref. [3]). As soon as it becomes kinematically possible to decay the heavy Higgs into a light Higgs pair, the ZZH coupling is already too small to generate a sizable cross section. Furthermore, the continuum MSSM cross section is suppressed with respect to the SM cross section since the MSSM couplings ZZH and ZZh vary with $\cos(\beta-\alpha)$ and $\sin(\beta-\alpha)$, respectively, with respect to the corresponding SM coupling. Notice that in this regime, at a LC, the λ_{hhh} vertex could in principle be accessible instead, since $\lambda_{hhh} \gg \lambda_{Hhh}$ (see Fig. 2 of Ref. [3]) and because of the kinematic enhancement induced by $m_h \ll m_H$. Unfortunately, we will see that the size of the $e^+e^- \to hhZ$ cross section itself is prohibitively small.

We assume that b-jets are distinguishable from light-quark and gluon jets and no efficiency to tag the four b-quarks is included in our parton level results. We further neglect considering the possibility of the b-jet charge determination. Also, to simplify the calculations, the Z boson appearing in the final state of the LC process is treated as on-shell and no branching

ratio (BR) is applied to quantify its possible decays. In practice, one may assume that it decays leptonically (i.e., $Z \to \ell^+\ell^-$, with $\ell = e, \mu, \tau$) or hadronically into light-quark jets (i.e., $Z \to q\bar{q}$, with $q \neq b$), in order to avoid problems with $6b$-quark combinatorics. Furthermore, in the LC analysis, we have not simulated the effects of Initial State Radiation (ISR), beamstrahlung or Linac energy spread. Indeed, we expect them to affect signal and backgrounds rather similarly, so we can neglect them for the time being. Indeed, since a detailed phenomenological study, including both hadronisation and detector effects, already exists for the case of double Higgs-strahlung in e^+e^- [4], whose conclusions basically support those attained in the theoretical study of Ref. [5], we limit ourselves here to update the latter to the case of the MSSM.

So far only resonant production $gg \to H \to hh \to b\bar{b}b\bar{b}$ has been investigated [10], with full hadronic and detector simulation and considering also the (large) QCD backgrounds, and a similar study does not exist for continuum double Higgs production at the LHC. (See Ref. [17] for a detailed account of the $gg \to H \to hh \to \gamma\gamma b\bar{b}$ decay channel.) The event simulation has been performed by using a special version of PYTHIA [18], in which the relevant LO MEs for double Higgs production of Ref. [11] have been implemented by M. El Kacimi and R. Lafaye. These MEs take into account both continuum and resonant double Higgs boson production and their interferences. (The insertion of those for e^+e^- processes is in progress.) The PYTHIA interface to HDECAY has been exploited in order to generate the MSSM Higgs mass spectrum and the relevant Higgs BRs, thus maintaining consistency with the parton level approach. As for the LHC detector simulation, the fast simulation package was used, with high luminosity (i.e., $\int \mathcal{L}dt = 100$ fb^{-1}) parameters.

The motivation for our study is twofold. On the one hand, to complement the studies of Ref. [10] by also considering the continuum production $gg \to hh \to b\bar{b}b\bar{b}$ at large $\tan\beta$. On the other hand, to explore the possibility of further kinematic suppression of the various irreducible backgrounds to the resonant channel at small $\tan\beta$.

3 Results

3.1 The LHC analysis

In our LHC analysis, following the discussion in Sect. 2, we focus most of our attention on the case $\tan\beta = 3$, with $m_A = 210$ GeV, although other combinations of these two MSSM parameters will also be considered. We further set $A = -\mu = 1$ TeV and take all sparticle masses (and other SUSY scales) to be as large as 1 TeV.

3.1.1 $gg \to hh \to b\bar{b}b\bar{b}$ at parton level

In our parton level analysis, we identify jets with the partons from which they originate (without smearing the momenta) and apply all cuts directly to the partons. We mimic the finite coverage of the LHC detectors by imposing a transverse momentum threshold on each of the four b-jets,

$$p_T(b) > 30 \text{ GeV} \tag{4}$$

and requiring their pseudorapidity to be

$$|\eta(b)| < 2.5. \tag{5}$$

Also, to allow for their detection as separate objects, we impose an isolation criterium among b-jets,

$$\Delta R(bb) > 0.4, \tag{6}$$

by means of the usual cone variable $\Delta R(ij) = \sqrt{\Delta\eta(ij)^2 + \Delta\phi(ij)^2}$, defined in terms of relative differences in pseudo-rapidity η_{ij} and azimuth ϕ_{ij} of the i-th and j-th b-jets.

As preliminary and very basic selection cuts (also to help the stability of the numerical integration), we have required that the invariant mass of the entire $4b$-system is at least twice the mass of the lightest MSSM Higgs boson (apart from mass resolution and gluon emission effects), e.g.,

$$m(bbbb) \geq 2m_h - 40 \text{ GeV}, \tag{7}$$

and that exactly two h-resonances are reconstructed, such that

$$|m(bb) - m_h| < 20 \text{ GeV}. \tag{8}$$

In doing so, we implicitly assume that the h scalar boson has already been discovered and its mass measured through some other channel, as we have already intimated in the Introduction.

After the above cuts have been implemented, we have found that the two $4b$-backgrounds proceeding through EW interactions are negligible compared to the pure QCD process. In fact, the constraints described in eqs. (7)–(8) produce the strongest suppression, almost completely washing out the relatively enhancing effects that the cuts in (4)–(6) have on the EW components of the backgrounds with respect to the pure QCD one, owning to the intermediate production of massive Z bosons in the former. In the end, the production rates of the three subprocesses scale approximately as their coupling strengths: i.e., $\mathcal{O}(\alpha_s^4) : \mathcal{O}(\alpha_s^2\alpha_{em}^2) : \mathcal{O}(\alpha_{em}^4)$. Therefore, in the reminder of our analysis, we will neglect EW effects, as they represent not more than a 10% correction to the QCD rates, which are in turn affected by much larger QCD K-factors. As for the pure QCD background itself, it hugely overwhelms the double Higgs signal at this stage. The cross section of the former is about 7.85 pb, whereas that of the latter is approximately 0.16 pb.

To appreciate the dominance of the m_h cuts, one may refer to Fig. 2, where the distributions in transverse momentum of the four p_T-ordered b-quarks (such that $p_T(b_1) > ... > p_T(b_4)$) of both signal and QCD background are shown. Having asked the four b-jets of the background to closely emulate the $gg \to hh \to b\bar{b}b\bar{b}$ kinematics, it is not surprising to see a 'degeneracy' in the shape of all spectra. Clearly, no further background suppression can be gained by increasing the $p_T(b)$ cuts. The same can be said for $\eta(b)$ and $\Delta R(bb)$. Others quantities ought to be exploited.

In Fig. 3, we present the signal and QCD background distributions in the minimum angle formed between the two b-quarks coming from the 'same Higgs' (i.e., those fulfilling the cuts in (8)) in the $4b$-system rest frame (the plot is rater similar for the maximum angle, thus

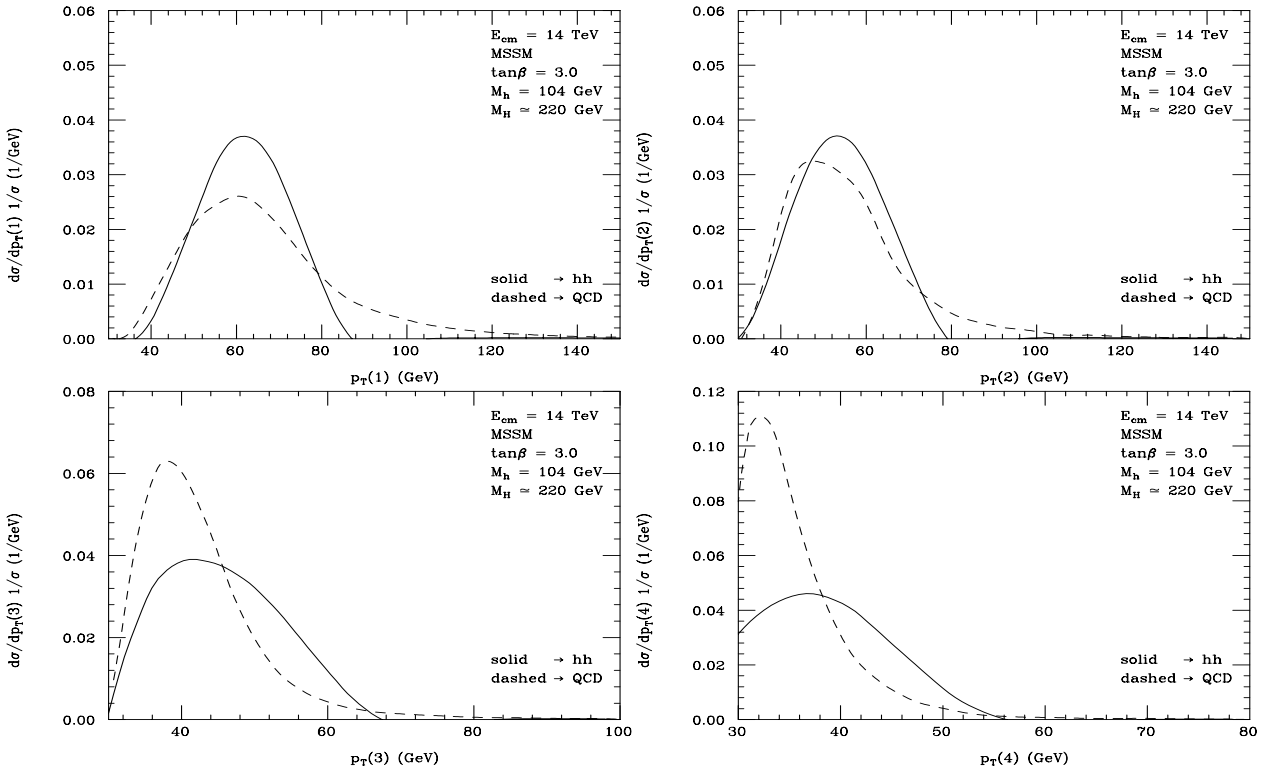

Figure 2: Distributions in transverse momentum of the four p_T-ordered b-jets in $gg \to hh \to b\bar{b}b\bar{b}$ and in the QCD background, after the cuts (4)–(8) at the LHC, for $\tan\beta = 3$, $m_h = 104$ GeV and $m_H \simeq 220$ GeV. Normalisation is to unity.

also on average). There, one can see a strong tendency of the two $2b$-pairs produced in the Higgs decays to lie back-to-back, reflecting the $2 \to 2$ intermediate dynamics of Higgs pair production via $gg \to hh$. Missing such kinematically constrained virtual state, the QCD background shows a much larger angular spread towards small $\theta_{\rm min}(bb)$ values, eventually tamed by the isolation cut (6).

The somewhat peculiar shape of the signal distribution is due to destructive interference. Recall that the signal contains not only diagrams proceeding via a heavy Higgs resonance (the upper-left hand graph of Fig. 1), which results in the large peak in Fig. 3, but also contains a continuum contribution mediated by box graphs (the upper-right hand graph of Fig. 1). These two contributions destructively interfere leading to the depletion of events between the large back-to-back peak and the small remaining 'bump' of the continuum contribution as seen in Fig. 3.

In the end, a good criterium to enhance the signal-to-background ratio (S/B) is to require, e.g., $\theta(bb) > 2.4$ radians, i.e., a separation between the $2b$-jets reconstructing the lightest Higgs boson mass of about 140 degrees in angle. (Incidentally, we also have investigated the angle that each of these $2b$-pairs form with the beam axis, but found no significant difference between signal and QCD background).

An additional consequence that one should expect from the presence of two intermediate massive objects in $gg \to hh \to b\bar{b}b\bar{b}$ events is the spherical appearance of the jets in the

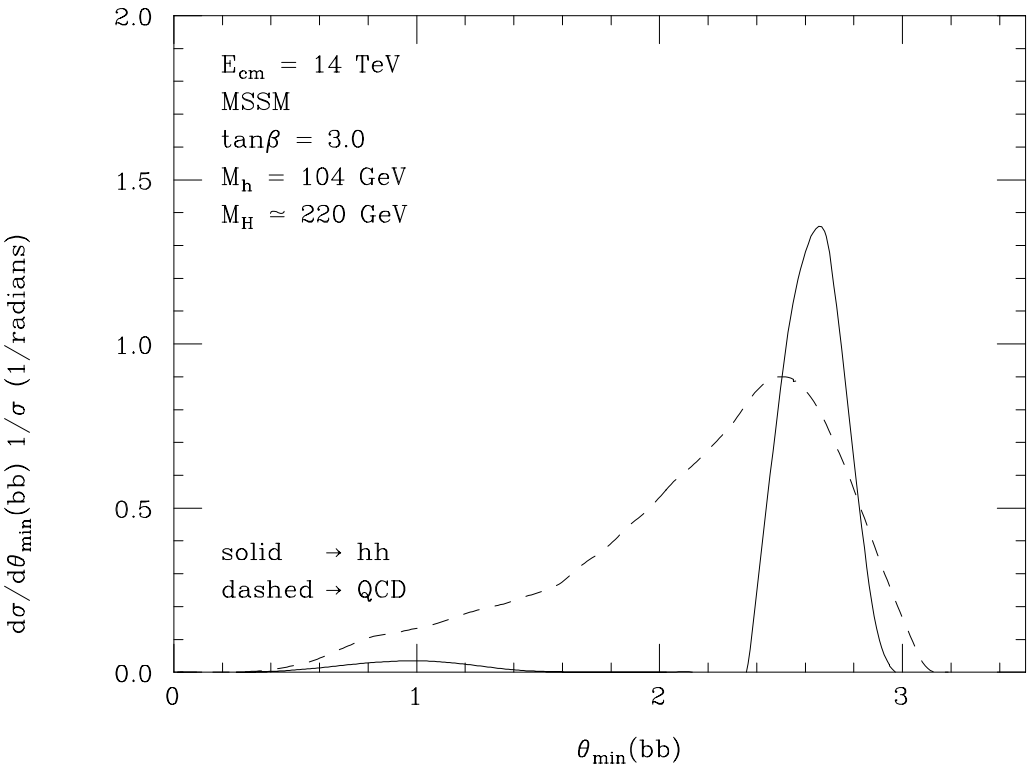

Figure 3: Distributions in minimum relative angle (in radians) in the $4b$-system rest frame between two b-jets reconstructing m_h in $gg \to hh \to b\bar{b}b\bar{b}$ and in the QCD background, after the cuts (4)–(8) at the LHC, for $\tan\beta = 3$, $m_h = 104$ GeV and $m_H \simeq 220$ GeV. Normalisation is to unity.

final state, in contrast to the usual planar behaviour of the infrared QCD interactions. These phenomena can be appreciated in Fig. 4. Notice there the strong tendency of the background to yield high thrust configurations, again controlled by the separation cuts when T approaches unity. On the contrary, the average value of the thrust in the signal is much lower, being the effect of accidental pairings of 'wrong' $2b$-pairs (the shoulder at high thrust values) marginal. An effective selection cut seems to be, e.g., $T < 0.85$.

Furthermore, if the heavy Higgs mass is sufficiently well measured at the LHC then one can exploit the large fraction [2] of $4b$-events which peak at m_H in the signal, as dictated by the $H \to hh$ decay, improving the signal-to-background ratio. This peak at m_H can be clearly seen in the left hand plot of Fig. 5, where it dominates the QCD background, even for bins 13 GeV wide. In fact, not only could the QCD background be considerably suppressed but also those contributions to $gg \to hh$ not proceeding through an intermediate H state should be removed, this greatly enhancing the sensitivity of the signal process to the λ_{Hhh} coupling. This can be seen in the right hand plot of Fig. 5 where the signal is shown on a logarithmic scale. The continuum contribution due to the box graphs (and its destructive interference with the heavy Higgs decay contribution) is now evident although one should note that it is considerably suppressed compared to the peak at m_H.

Now, if a less than 10% mass resolution can be achieved on the light and heavy Higgs

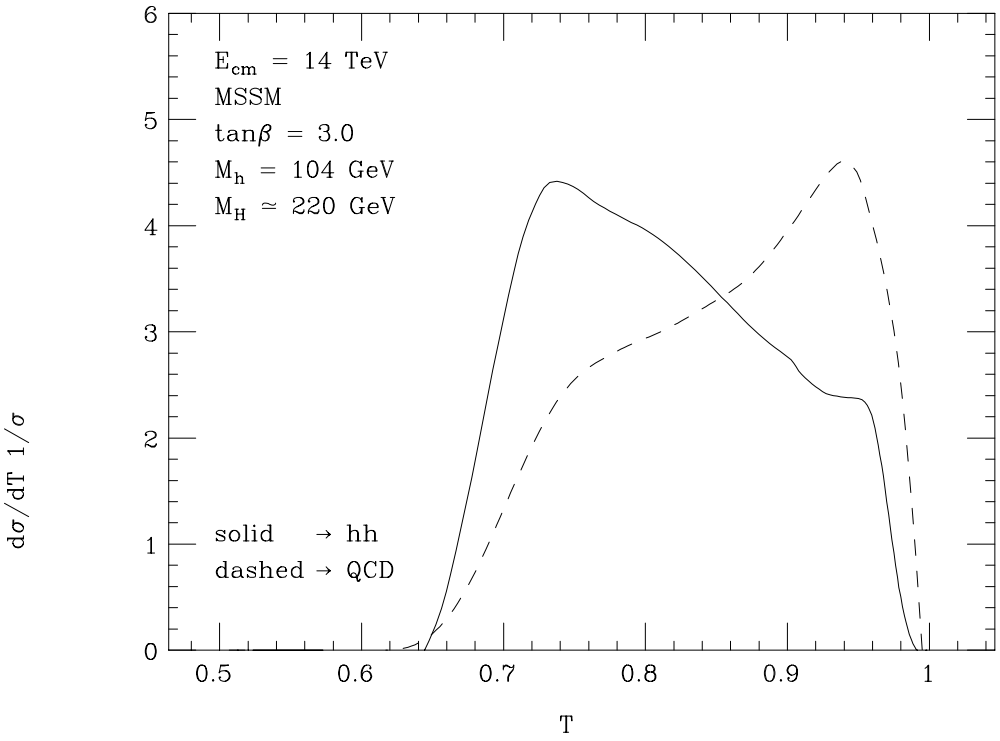

Figure 4: Distributions in thrust in the rest frame of the 4b-system in $gg \to hh \to b\bar{b}b\bar{b}$ and in the QCD background, after the cuts (4)–(8) at the LHC, for $\tan\beta = 3$, $m_h = 104$ GeV and $m_H \simeq 220$ GeV. Normalisation is to unity.

masses, then one can tighten cut (8) to $|m(bb) - m_h| < 10$ GeV and introduce the additional cut $|m(bbbb) - m_H| < 20$ GeV. These cuts taken together with those in $\theta(bb)$ and T already suggested, reduce the QCD background to the same level as the signal. In fact, we have found that the cross section of the background drops to approximately 174 fb whereas that of the signal remains as large as 126 fb, this yielding a very high statistical significance at high luminosity. Even for less optimistic mass resolutions the signal-to-background ratio is still significantly large. For example, selecting events with $|m(bb) - m_h| < 20$ GeV and $|m(bbbb) - m_H| < 40$ GeV, the corresponding numbers are approximately 102 fb for the signal and 453 fb for the background. Notice that the signal actually decreases as these Higgs mass windows are made larger. This is due to our insistence that exactly two $b\bar{b}$ pairs should reconstruct the light Higgs mass. As the light Higgs mass window is enlarged from $m_h \pm 10$ GeV to $m_h \pm 20$ GeV, it becomes more likely that accidental pairings reconstruct the light Higgs boson. Since one is then unable to unambiguously assign the b quarks to the light Higgs bosons, the event is rejected and the signal drops.

Although we have discussed here an ideal situation which is difficult to match with more sophisticated hadronic and detector simulations, it still demonstrates that the measurement of the λ_{Hhh} coupling could be well within the potential of the LHC, at least for our particular choice of MSSM parameters. Comforted by such a conclusion, we now move on to more realistic studies.

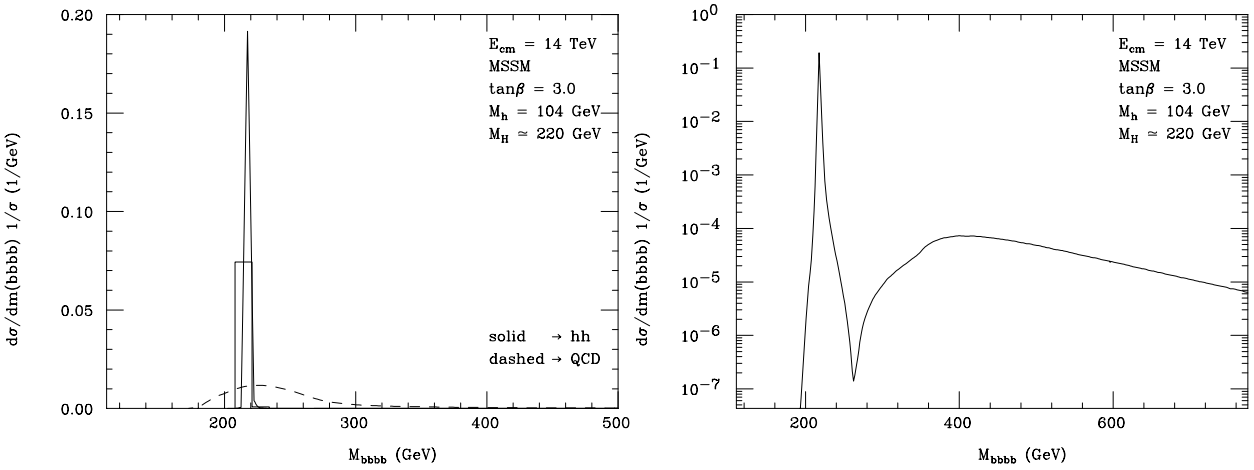

Figure 5: Distributions in invariant mass of the 4b-system in $gg \to hh \to b\bar{b}b\bar{b}$ and in the QCD background, after the cuts (4)–(8) at the LHC, for $\tan\beta = 3$, $m_h = 104$ GeV and $m_H \simeq 220$ GeV. Normalisation is to unity. The left hand plot shows both the signal (solid curve) and the QCD background (dashed curve), distributed in 5 GeV bins. The same signal is also shown as a histogram for a more experimentally realistic binning of 13 GeV. The right hand plot also shows the signal (collected in 5 GeV wide bins) on a logarithmic scale. Here the structure of the continuum contribution (and its destructive interference with the heavy Higgs decay contribution) can be seen.

3.1.2 $gg \to hh \to b\bar{b}b\bar{b}$ at the LHC experiments

Although the LHC experiments will be the first where one can attempt to measure the Higgs self-couplings, the analysis is very challenging because of the smallness of the production cross sections. Even in the most favourable cases, the production rate is never larger than a few picobarns, already including one-loop QCD corrections, as computed in Ref. [11]. The cross sections at this accuracy are given in Tab. 1, for the resonant process (case 1 with $m_H = 220$ GeV) as well as three non resonant scenarios: one at the same $\tan\beta$ but with the $H \to hh$ decay channel closed (case 2), a second at very large $\tan\beta$ and no visible resonance (case 3) and, finally, the SM option (case 4, where m_h identifies with the mass of the standard Higgs state).

case	model	$\tan\beta$	m_h (GeV)	A (TeV)	μ (TeV)	σ (fb)	dominant mode
1	MSSM	3	104	+1	−1	2000	$gg \to H \to hh$
2	MSSM	3	100	+1	−1	20	$gg \to hh$
3	MSSM	50	105	+1	+1	5000	$gg \to hh$
4	SM	-	105	-	-	40	$gg \to hh$

Table 1: Cross sections for double Higgs production hh at the LHC via gluon-gluon fusion at NLO accuracy, for three possible configurations of the MSSM and in the SM as well.

3.1.3 LHC trigger acceptance

For $4b$-final states, possible LHC triggers are high p_T electron/muons and jets. As an example, the foreseen ATLAS level 1 trigger thresholds on p_T and acceptance for a $4b$-selection (with the four b-jets reconstructed in the detector) are given in Tab. 2, assuming the LHC to be running at high luminosity.

trigger type: p_T in GeV	1 e 30	1 μ 20	2 μ 10	1 jet 290	3 jets 130	4 jets 90	total
case 1, $\epsilon(bbbb)$ in %	0.01	0.01	0.4	0.08	0.08	0.05	0.53
case 2	< 0.01	< 0.01	2.1	2.9	3.8	4.2	8.8
case 3	< 0.01	< 0.01	2.2	2.7	3.8	4.1	8.7
case 4	< 0.01	< 0.01	2.0	2.5	3.3	3.6	7.8

Table 2: Kinematical acceptance of the ATLAS detector to trigger four b-jets (including detector acceptance) at high luminosity.

The overall trigger acceptance is at best 8–9%, for cases 2,3,4. The very low efficiency for case 1 is clearly a consequence of the small value of the difference $m_H - 2m_h$, translating into a softer $p_T(b)$ spectrum with respect to the other cases (compare the left-hand with the right-hand side of Fig. 6). One can further see in the left-hand plot of Fig. 6 that the bulk of the signal lies below the lowest $p_T(b)$ threshold of Tab. 2 (i.e., 90 GeV), so that adopting smaller trigger thresholds could result in a dramatic enhancement of our efficiency. Of course, this would also substantially increase the low transverse momentum QCD background, as we can see in the parton level analysis of Fig. 2.

For example, by lowering the thresholds to 180, 80 and 50 GeV for 1, 3 and 4 jets, respectively (compare to Tab. 2), the overall trigger acceptance on the signal goes up to 1.8%, i.e., by almost a factor of 4. Meanwhile though, the ATLAS level-1 jet trigger rates increase by a factor of 10 [19]. Anyhow, even for our poor default value of $\epsilon(bbbb)$ in Tab. 2, we will see that case 1 still yields a reasonable number of events in the end. Optimisations of the b-jet transverse momentum thresholds are in progress [6].

3.1.4 LHC events selection for $gg \to hh \to b\bar{b}b\bar{b}$

Jets are reconstructed merging tracks inside $\Delta R(bb) = 0.4$. Only jets with transverse energy/momentum greater than 30 GeV and with $|\eta(b)| < 2.5$ are kept. (Thus, the same cuts as in the parton level analysis, now applied instead to jets.) The effect from pile up is included in the resolution. A jet energy correction is then applied.

The invariant masses of each jet pair can then be computed. Assuming that the lightest Higgs boson mass is known, events with $m(bb)$ sufficiently close to m_h can efficiently be selected, see Fig. 7. Another cut on the $\Delta R(bb, bb)$ between pairs of b-jets can also be applied to reduce the intrinsic combinatorial background, since the latter concentrates at large $\Delta R(bb, bb)$ values, see Fig. 8.

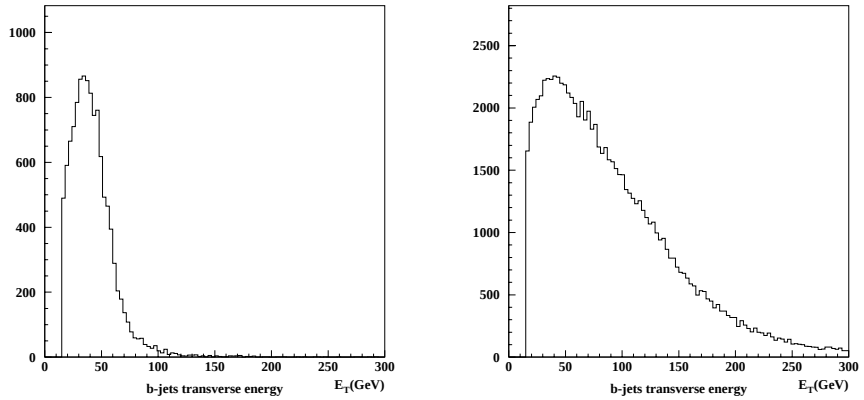

Figure 6: Reconstructed transverse energy/momentum for b-jets in $gg \to hh \to b\bar{b}b\bar{b}$ events of case 1 (left plot) and b-jets in $gg \to hh \to b\bar{b}b\bar{b}$ events of case 2 (right plot) with ATLAS fast simulation [20] at high luminosity. Normalisation is arbitrary.

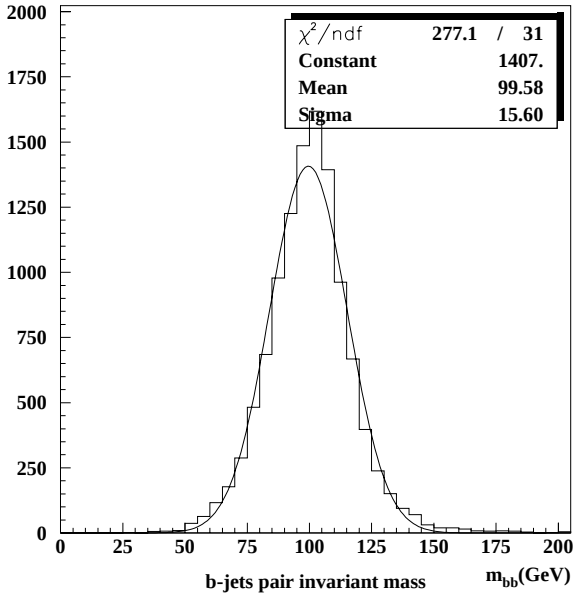

Figure 7: Reconstructed invariant mass distribution of $2b$-jet pairs in continuum $gg \to hh \to b\bar{b}b\bar{b}$ events (case 2) with the fast simulation at high luminosity. Normalisation is arbitrary. (Results of a Gaussian fit are also given.)

For case 1, as already discussed, we can further impose that the invariant mass of the four b-jets should be the heavy Higgs mass, m_H, in order to select the $H \to hh$ resonance, as confirmed by Fig. 9. In the other three cases, where the $H \to hh$ splitting is no longer dominant (MSSM) or non-existent (SM), one can still insist that the $4b$-jet invariant mass should be higher than two times the lightest Higgs mass, see Fig. 10 and recall eq. (7). Finally, following Fig. 11, by constraining the b-jets pairs four-momenta around the known

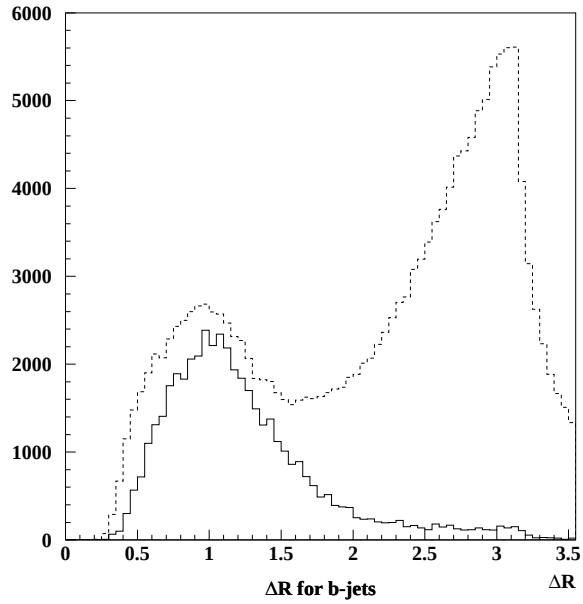

Figure 8: Reconstructed $\Delta R(bb, bb)$ between $2b$-jet systems from $h \to bb$ decays in continuum $gg \to hh \to b\bar{b}b\bar{b}$ events (case 2) with the fast simulation at high luminosity. The dashed histogram shows the same distribution for all pairs of jets. Normalisation is arbitrary.

light Higgs mass value, m_h, one can further reject the intrinsic background by means of the $m(bbbb)$ spectrum.

3.1.5 LHC b-tagging in $gg \to hh \to b\bar{b}b\bar{b}$

The b-tagging efficiency at high luminosity is set to 50%, with p_T dependent correction factors for jets rejection. An average rejection of 10 for c-jets and 100 for light-jets can be expected. We then studied the effect on the selection efficiency of requiring from one to four b-tags, although it is clear that, according to the parton level studies, the huge background rate demands four b-tags, leading to a 6% tagging efficiency overall.

3.1.6 Event rates at the LHC

Taking into account all the efficiencies described above, and using the NLO normalisation of Tab. 1, one can extract the number of expected events per year at the LHC at high luminosity given in Tab. 3. The selection cuts enforced here are the following. For a start, we have kept configurations where $|m(bb) - m_h| < 30$ GeV (cases 1,3,4) or $|m(bb) - m_h| < 20$ GeV (case 2) and $\Delta R(bb, bb) < 2.5$ (all four cases). (If more than two m_h's are reconstructed, the best two $2b$-pairs are selected according to the minimum value of $\delta M^2 = [m_h - m(bb)]^2 + [m_h - m'(bb)^2]$.) Then, a cut on $m(bbbb)$ is applied: in presence of the $H \to hh$ resonance (case 1) we have kept events within an m_H mass window of $\pm 2\sigma$ (about 82% of the total number survive);

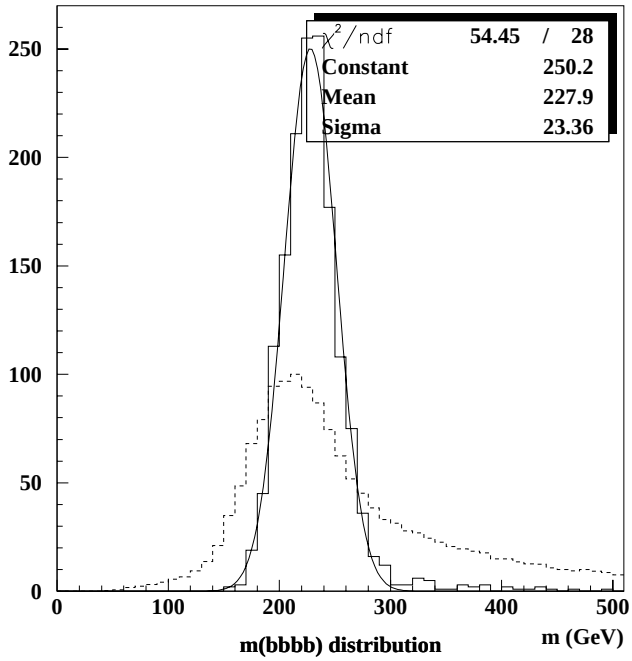

Figure 9: Reconstructed 4b-jet invariant mass for b-jets coming from the hh pair in $gg \to hh \to b\bar{b}b\bar{b}$ events (case 1) with the fast simulation at high luminosity. The dashed histogram shows the same distribution for all groups of four jets. Normalisation is arbitrary. (Results of a Gaussian fit to the first spectrum are also given.)

otherwise (cases 2,3,4) we have adjusted the $m(bbbb) \gtrsim 2m_h$ cut so to keep 90% of the sample. In the end, one finds the numbers in Tab. 3, that are encouraging indeed.

	case 1	2	3	4
σ in fb	2000	20	5000	40
trigger threshold acceptance	0.53%	8.8%	8.7%	7.8%
mass windows	60%	50%	40%	40%
4b-tagging	6%	6%	6%	6%
events/year (no tagging)	636	88	17400	125
events/year (four b-tags)	38	5.3	1044	7.5

Table 3: Total rates for $gg \to hh \to b\bar{b}b\bar{b}$, after all efficiencies have been included and selection cuts (4)–(6) enforced at hadron level, with 100 fb^{-1} per year of luminosity.

In conclusion then, looking at the results in Tab. 3 and bearing in mind the potential seen in reducing the pure QCD background via $gg \to \mathcal{O}(\alpha_s^4) \to b\bar{b}b\bar{b}$ (see Figs. 3–5), one should be confident in the LHC having the potential to measure the λ_{Hhh} coupling in resonant $H \to hh$ events (case 1). To give more substance to such a claim, we have now initiated background

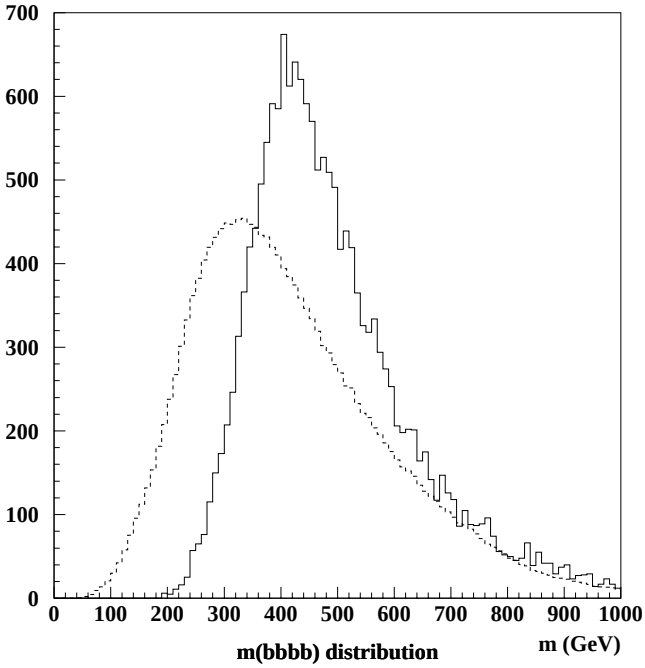

Figure 10: Reconstructed 4b-jet invariant mass for b-jets coming from the hh pair in $gg \to hh \to b\bar{b}b\bar{b}$ events (case 4) with the fast simulation at high luminosity. The dashed histogram shows the same distribution for all groups of four jets. Normalisation is arbitrary.

studies at hadron and detector level, following the guidelines obtained by the parton level analysis [6]. As for other configurations of the MSSM (such as case 2) or in the SM (case 4), the expectations are more pessimistic. Case 3 deserves further attention. In fact, notice the large number of events surviving and recall what mentioned in the Introduction concerning the potential of the non-resonant $gg \to hh \to b\bar{b}b\bar{b}$ process as a discovery channel of the light Higgs boson of the MSSM in the large $\tan\beta$ region at moderate m_A values, a corner of the parameter space where the h coverage is given only by SM-like production/decay modes, thus not allowing one to access information on the MSSM parameters. Results on this topic too will be presented in Ref. [6].

3.2 The LC analysis

Here, we closely follow the selection procedure advocated in Ref. [5]. In order to resolve the four b-jets as four separate systems inside the LC detector region, we impose the following cuts. First, that the energy of each b-jet is above a minimum threshold,

$$E(b) > 10 \text{ GeV}. \tag{9}$$

Second, that any b-jet is isolated from all others, by requiring a minimum angular separation,

$$\cos\theta(b,b) < 0.95. \tag{10}$$

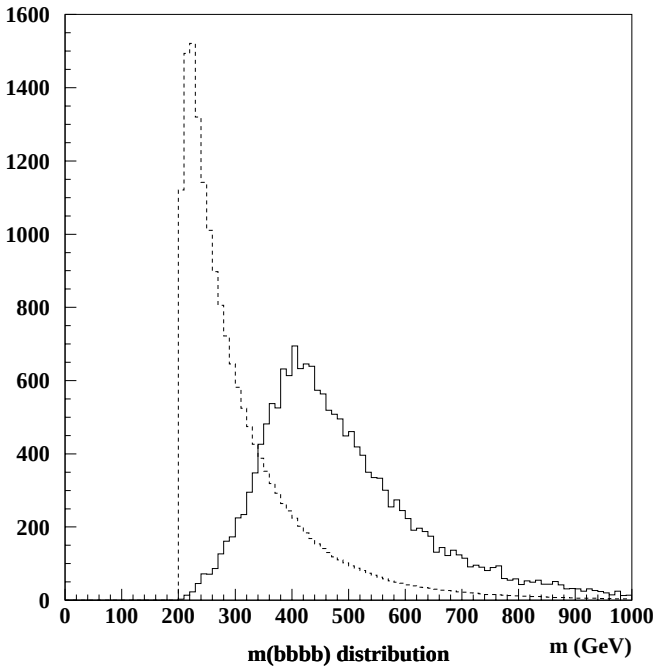

Figure 11: Reconstructed 4b-jet invariant mass for b-jets coming from the hh pair in $gg \to hh \to b\bar{b}b\bar{b}$ events (case 4) with the fast simulation at high luminosity. Here, the energy of the jet pairs is recalculated using the m_h constraint. The dashed histogram shows the same distribution for all groups of four jets. Normalisation is arbitrary.

Similarly to the hadronic analysis, one can optimise S/B by imposing the constraints [5],

$$m(bbbb) \geq 2m_h - 10 \text{ GeV}, \tag{11}$$

$$|m(bb) - m_h| < 5 \text{ GeV}, \tag{12}$$

on exactly two combinations of 2b-jets. Here, note that the mass resolution adopted for the quark systems is significantly better than in the LHC case, due to the cleanliness of the e^+e^- environment and the expected performance of the LC detectors in jet momentum and angle reconstruction [21]. Thus, given such high mass resolution power from the LC detection apparatus, one may further discriminate between h and Z mass peaks by requiring that none of the 2b-jet pairs falls around m_Z,

$$|m(bb) - m_Z| > 5 \text{ GeV}. \tag{13}$$

Moreover, in the double Higgs-strahlung process $e^+e^- \to hhZ$, the four b-quarks are produced centrally, whereas this is generally not the case for the background (see the discussion in Ref. [5]). This can be exploited by enforcing

$$|\cos\theta(bb, bbb, bbbb)| < 0.75, \tag{14}$$

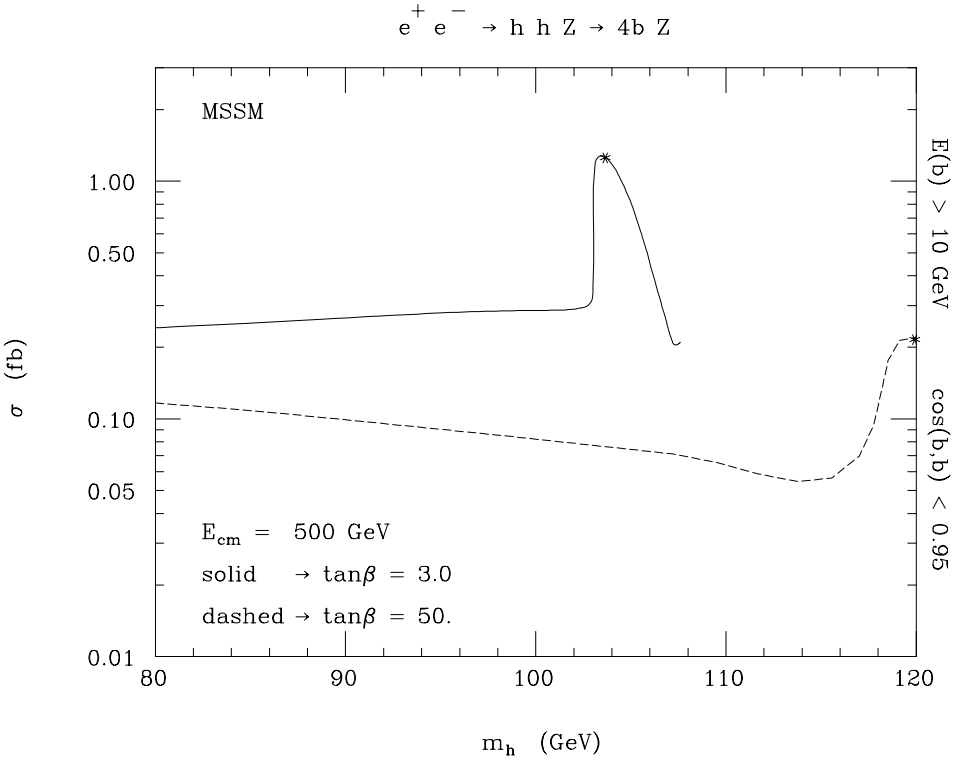

Figure 12: Cross sections in femtobarns for the $e^+e^- \to hhZ$ signal in the $h \to b\bar{b}b\bar{b}$ decay channel, at a LC with 500 GeV as CM energy, as a function of m_h for $\tan\beta = 3$ and 50. Our acceptance cuts in energy and separation of the four b-quarks (9)–(10) have been implemented. No beam polarisation is included.

where $\theta(bb, bbb, bbbb)$ are the polar angles of all two-, three- and four-jet systems.

Fig. 12 shows the production and decay rates of the signal process, $e^+e^- \to hhZ \to b\bar{b}b\bar{b}Z$, as obtained at the partonic level, after the cuts (9)–(10) have been implemented. The MSSM setup here includes some mixing, having adopted $A = 2.4$ TeV and $\mu = 1$ TeV, at both $\tan\beta = 3$ and 50. Notice the onset of the $H \to hh \to b\bar{b}b\bar{b}$ decay sequence in the Higgs-strahlung process $e^+e^- \to HZ$ at low $\tan\beta$. The same does not occur for large values, as previously explained. The impact of the above jet selection cuts on the signal is marginal, as the b-quarks are here naturally isolated and energetic, being the decay products of heavy objects. In fact, the rates in Fig. 12 would only be 10–20% higher if all the $4b$-quark phase space was allowed (the suppression being larger for smaller Higgs masses). At the height of the resonant peak around $m_h \approx 104$ GeV at $\tan\beta = 3$, the signal rate is not large but observable, yielding more than one event every 1 fb^{-1} of data. For a high luminosity 500 GeV TESLA design [22], this would correspond to more than 300 events per year. Given the very high efficiency expected in tagging b-quark jets, estimated at 90% for each pairs of heavy quarks [23], one should expect a strong sensitivity to the triple Higgs self-coupling. The situation at large $\tan\beta$ is much more difficult instead, being the production rates smaller by about a factor of 10.

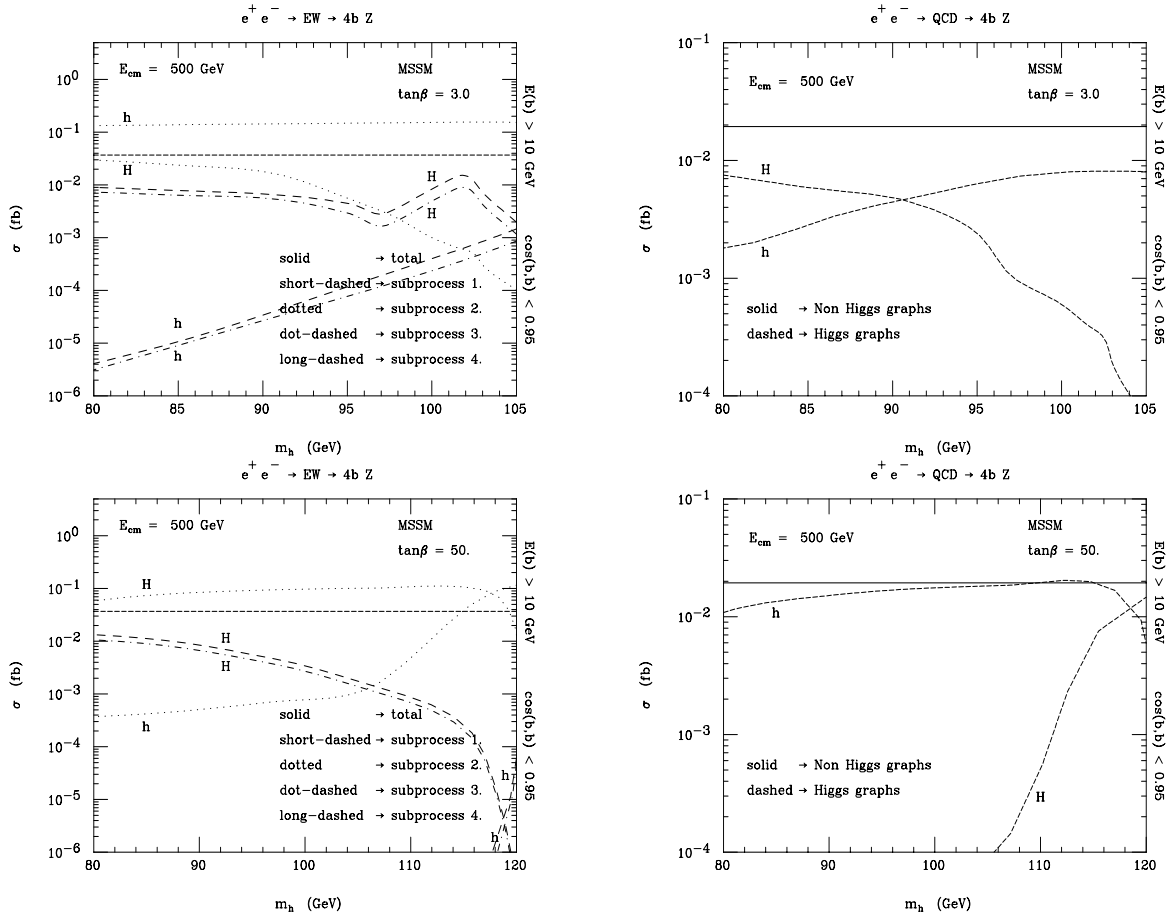

Figure 13: Cross sections in femtobarns for the dominant components of the EW (left) and EW/QCD (right) background to the $e^+e^- \to hhZ$ signal in the $h \to b\bar{b}b\bar{b}$ decay channel, at a LC with 500 GeV as CM energy, as a function of m_h for $\tan\beta = 3$ (top) and 50 (bottom). Our acceptance cuts in energy and separation of the four b-quarks (9)–(10) have been implemented. No beam polarisation is included.

In the left-hand side of Fig. 13 we present the EW background, after the constraints in (9)–(10) have been enforced, in the form of the four dominant EW sub-processes. These four channels are the following.

1. $e^+e^- \to ZZZ \to b\bar{b}b\bar{b}Z$, first from the left in the second row of topologies in Fig. 3 of Ref. [5]. That is, triple Z production with no Higgs boson involved.

2. $e^+e^- \to h/HZZ \to b\bar{b}b\bar{b}Z$, first(first) from the left(right) in the fifth(fourth) row of topologies in Fig. 2 of Ref. [5] (also including the diagrams in which the on-shell Z is connected to the electron-positron line). That is, single Higgs-strahlung production in association with an additional Z, with the Higgs decaying to $b\bar{b}$. The cross sections of these two channels are obviously identical.

3. $e^+e^- \to h/HZ \to Z^*Z^*Z \to b\bar{b}b\bar{b}Z$, first from the right in the third row of topologies

in Fig. 2 of Ref. [5]. That is, single Higgs-strahlung production with the Higgs decaying to $b\bar{b}b\bar{b}$ via two off-shell Z^* bosons.

4. $e^+e^- \to Zh/H \to b\bar{b}Z^*Z \to b\bar{b}b\bar{b}Z$, first(first) from the right(left) in the first(second) row of topologies in Fig. 2 of Ref. [5]. That is, two single Higgs-strahlung production channels with the Higgs decaying to $b\bar{b}Z$ via one off-shell Z^* boson. Also the cross sections of these two channels are identical to each other, as in 2.

The $\mathcal{O}(\alpha_s^2\alpha_{em}^3)$ EW/QCD background is dominated by $e^+e^- \to ZZ$ production with one of the two Z bosons decaying hadronically into four b-jets. This subprocess corresponds to the topology in the middle of the first row of diagrams in Fig. 4 of Ref. [5]. Notice that Higgs graphs are involved in this process as well (bottom-right topology in the mentioned figure of [5]). These correspond to single Higgs-strahlung production with the Higgs scalar subsequently decaying into $b\bar{b}b\bar{b}$ via an off-shell gluon. Their contribution is not entirely negligible, owing to the large ZH production rates, as can be seen in the right-hand side of Fig. 13. The interferences among non-Higgs and Higgs terms are always negligible.

In performing the signal-to-background analysis, we have chosen two representative points only, identified by the two following combinations: (i) $\tan\beta = 3$ and $m_A = 210$ GeV (yielding $m_h \approx 104$ GeV and $m_H \approx 220$ GeV); (ii) $\tan\beta = 50$ and $m_A = 130$ GeV (yielding $m_h \approx 120$ GeV and $m_H \approx 130$ GeV). These correspond to the two asterisks in Fig. 12, that is, the maxima of the signal cross sections at both $\tan\beta$ values. The first corresponds to resonant $H \to hh$ production, whereas the latter to the continuum case. If we enforce the constraints of eq. (11)–(14), the suppression of both EW and EW/QCD is enormous, so that the corresponding cross sections are of $\mathcal{O}(10^{-3})$ fb, while the signal rates only decrease by a factor of four at most. This is the same situation that was seen for the SM case in Ref. [5]. Indeed, in the end it is just a matter of how many signal events survive, the sum of the backgrounds representing no more than a 10% correction (see Fig. 11 of Ref. [5]). For example, after 500 fb^{-1} of data collected, one is left with 156 and 15 events for case (i) and (ii), respectively. However, these numbers do not yet include b-tagging efficiency and Z decay rates.

4 Summary

To summarise, the 'double Higgs production' subgroup has contributed to the activity of the Higgs WG by assessing the feasibility of measurements of triple Higgs self-couplings at future TeV colliders. The machines considered were the LHC at CERN (14 TeV) and a future LC running at 500 GeV. In both cases, a high luminosity setup was assumed, given the smallness of the double Higgs production cross sections. In particular, the $H \to hh$ resonant enhancement was the main focus of our studies, involving the lightest, h, and the heaviest, H, of the neutral Higgs bosons of the MSSM, in the kinematic regime $m_H \gtrsim 2m_h$. This dynamics can for example occur in the following reactions: $gg \to hh$ in the hadronic case and $e^+e^- \to hhZ$ in the leptonic one, but only at low $\tan\beta$. These two processes proceed via intermediate stages of the form $gg \to H$ and $e^+e^- \to HZ$, respectively, followed

by the decay $H \to hh$. Thus, they in principle allow one to determine the strength of the Hhh vertex involved, λ_{Hhh}, in turn constraining the form of the MSSM Higgs potential itself. The signature considered was $hh \to b\bar{b}b\bar{b}$, as the $h \to b\bar{b}$ decay rate is always dominant.

We have found that several kinematic cuts can be exploited in order to enhance the signal-to-background rate to level of high significance, particularly at the e^+e^- machine. At the pp accelerator, in fact, the selection of the signal is made much harder by the presence of an enormous background in $4b$ final states due to pure QCD. In parton level studies, based on the exact calculation of LO scattering amplitudes of both signals and backgrounds (without any showering and hadronisation effects but with detector acceptances), we have found very encouraging results. At a LC, the double Higgs signal can be studied in an essentially background free environment. At the LHC, the signal and the QCD background are in the end at the same level with detectable but not very large cross sections.

Earlier full simulations performed for the e^+e^- case had already indicated that a more sophisticated treatment of both signal and backgrounds, including fragmentation/hadronisation and full detector effects, should not spoil the results seen at the parton level. For the LHC, our preliminary studies of $gg \to H \to hh \to b\bar{b}b\bar{b}$ in presence of the $gg \to hh \to b\bar{b}b\bar{b}$ continuum (and relative interferences) also point to the feasibility of the signal selection, after realistic detector simulation and event reconstruction. As for double h production in the continuum, although not very useful for Higgs self-coupling measurements, this seems a promising channel, if not to discover the lightest MSSM Higgs boson certainly to study its properties and those of the Higgs sector in general (because of the large production and decay rates at high $\tan\beta$ and its sensitivity to such a parameter), as shown from novel simulations also presented in this study. (The discovery potential of this mode will eventually be addressed in Ref. [6].) Despite lacking a full background analysis in the LHC case, we have no reason to believe that a comparable degree of suppression of background events seen at parton level cannot be achieved also at hadron level. Progress in this respect is currently being made [6].

Acknowledgements

SM acknowledges financial support from the UK-PPARC. The authors thank Patrick Aurenche and the organisers of the Workshop for the stimulating environment that they have been able to create. DJM and MM thank Michael Spira for useful discussions. Finally, we all thank Elzbieta Richter-Was for many useful comments and suggestions.

References

[1] For an incomplete list of references, see:
G. Gounaris, D. Schildknecht and F. Renard, Phys. Lett. **B83** (1979) 191; Erratum, *ibidem* **B89** (1980) 437; V. Barger, T. Han and R.J.N. Phillips, Phys. Rev. **D38** (1988) 2766; V.A. Ilyin, A.E. Pukhov, Y. Kurihara, Y. Shimizu and T. Kaneko, Phys. Rev. **D54** (1996) 6717; F. Boudjema and E. Chopin, Z. Phys. **C71** (1996) 431. V. Barger and T. Han, Mod. Phys. Lett. **A5** (1990) 667; A. Dobrovolskaya and V. Novikov, Z. Phys.

C52 (1991) 427; D.A. Dicus, K.J. Kallianpur and S.S.D. Willenbrock, Phys. Lett. **B200** (1998) 187; A. Abbasabadi, W.W. Repko, D.A. Dicus and R. Vega, Phys. Rev. **D38** (1998) 2770; Phys. Lett. **B213** (1998) 386; E.W.N. Glover and J.J. van der Bij, Nucl. Phys. **B309** (1988) 282; T. Plehn, M. Spira and P.M. Zerwas, Nucl. Phys. **B479** (1996) 46; Erratum, *ibidem* **B531** (1998) 655; O. Brein and W. Hollik, preprint KA-TP-11-99, August 1999, `hep-ph/9908529`; G. Jikia, Nucl. Phys. **B412** (1994) 57; A. Djouadi, H.E. Haber and P.M. Zerwas, Report DESY 96–123D, `hep-ph/9605437`; P. Osland and P.N. Pandita, Phys. Rev. **D59** (1999) 055013; preprint BERGEN-1999-01, February 1999, `hep-ph/9902270`; to appear in the Proceedings of "XIVth International Workshop: High Energy Physics and Quantum Field Theory (QFTHEP99)", Moscow, Russia, 27 May - 2 June 1999, November 1999, `hep-ph/9911295`; P. Osland, preprint ISSN 0803-2696, March 1999, `hep-ph/9903301`.

[2] A. Djouadi, W. Kilian, M. Mühlleitner and P.M. Zerwas, Eur. Phys. J. **C10** (1999) 45.

[3] A. Djouadi, W. Kilian, M. Mühlleitner and P.M. Zerwas, Eur. Phys. J. **C10** (1999) 27; preprint DESY 99/171, PM/99-55, TTP99-48, January 2000, `hep-ph/0001169`.

[4] P. Lutz, talk given at the ECFA/DESY Workshop on "Physics and Detectors for a Linear Collider", Oxford, UK, 20-23 March 1999.

[5] D.J. Miller and S. Moretti, preprint RAL-TR-1999-032, June 1999, `hep-ph/9906395`; preprint RAL-TR-1999-073, Nov. 1999, talk at the ECFA/DESY Workshop on "Physics and Detectors for a Linear Collider", Oxford, UK, 20-23 March 1999, `hep-ph/0001194`.

[6] D.J. Miller, S. Moretti, M. Mühlleitner and R. Lafaye, in preparation.

[7] M. Carena, J.R. Espinosa, M. Quiros and C.E.M. Wagner, Phys. Lett. **B335** (1995) 209; M. Carena, M. Quiros and C.E.M. Wagner, Nucl. Phys. **B461** (1996) 407; H.E. Haber, R. Hempfling and A.H. Hoang, Z. Phys. **C75** (1997) 539; S. Heinemeyer, W. Hollik and G. Weiglein, Eur. Phys. J. **C9** (1999) 343; Phys. Lett. **B455** (1999) 179.

[8] E. Richter-Was *et al.*, Int. J. Mod Phys. **A13** (1998) 1371; E. Richter-Was and D. Froidevaux, Z. Phys. **C76** (1997) 665; J. Dai, J.F. Gunion and R. Vega, Phys. Lett. **B371** (1996) 71; *ibidem* **B378** (1996) 801.

[9] S. Moretti and W.J. Stirling, Phys. Lett. **B347** (1995) 291; Erratum, *ibidem* **B366** (1996) 451; A. Djouadi, J. Kalinowski and P.M. Zerwas, Z. Phys. **C70** (1996) 435; E. Ma, D.P. Roy and J. Wudka, Phys. Rev. Lett. **80** (1998) 1162.

[10] ATLAS Collaboration, ATLAS Detector and Physics Performance TDR CERN-LHCC/99-15 (May 25 1999); E. Richter-Was and D. Froidevaux, in Ref. [8].

[11] S. Dawson, S. Dittmaier and M. Spira, Phys. Rev. **D58** (1998) 115012.

[12] T. Stelzer and W.F. Long, Comp. Phys. Comm. **81** (1994) 357.

[13] H. Murayama, I. Watanabe and K. Hagiwara, HELAS: HELicity Amplitude Subroutines for Feynman Diagram Evaluations, KEK Report 91-11, January 1992.

[14] H.E. Haber and R. Hempfling, Phys. Rev. Lett. **66** (1991) 1815; Y. Okada, M. Yamaguchi and T. Yanagida, Prog. Theor. Phys. **85** (1991) 1; J. Ellis, G. Ridolfi and F. Zwirner, Phys. Lett. **B257** (1991) 83.

[15] A. Djouadi, H.E. Haber and P.M. Zerwas, Phys. Lett. **B375** (1996) 203.

[16] A. Djouadi, J. Kalinowski and M. Spira, Comput. Phys. Comm. **108** (1998) 56.

[17] E. Richter-Was *et al.*, ATLAS Note PHYS-No-074, 1996; in Ref. [8].

[18] T. Sjöstrand, Comp. Phys. Commun. **82** (1994) 74.

[19] A. Amadon *et al.*, ATLAS Internal Note DAQ-NO-108 (1998).

[20] E. Richter-Was *et al.*, ATLAS Note ATL-COM-PHYS-98-011.

[21] F. Richard, private communication.

[22] See, e.g.:
`http://www.desy.de/~njwalker/ecfa-desy-wg4/parameter_list.html`.

[23] G. Borissov, talk delivered at the ECFA/DESY Workshop on "Physics and Detectors for a Linear Collider", Oxford, UK, March 20–23, 1999; M. Battaglia, *ibidem.*